Solar-Terrestrial Physics. 2025, vol. 11, iss. 3, pp. 37–43. DOI: 10.12737/stp-113202505. © 2025 O.A. Danilova, N.G. Ptitsyna, V.E. Sdobnov. Published by INFRA-M Academic Publishing House

DOI: 10.12737/stp-113202505

Received March 10, 2025
Accepted May 30, 2025

GEOMAGNETIC CUTOFF OF COSMIC RAYS DURING THE MARCH 23–24, 2023 MAGNETIC STORM: RELATIONSHIP WITH SOLAR WIND PARAMETERS AND GEOMAGNETIC ACTIVITY TAKING INTO ACCOUNT LATITUDINAL EFFECTS

O.A. Danilova
Pushkov Institute of Terrestrial Magnetism, Ionosphere, and Radio Wave Propagation, St. Petersburg Branch RAS, St. Petersburg, Russia, md1555@mail.ru

N.G. Ptitsyna†
Pushkov Institute of Terrestrial Magnetism, Ionosphere, and Radio Wave Propagation, St. Petersburg Branch RAS, St. Petersburg, Russia

V.E. Sdobnov
Institute of Solar-Terrestrial Physics SB RAS, Irkutsk, Russia, sdobnov@mail.ru

Abstract. In this paper, we calculate geomagnetic cutoff rigidities during the strong magnetic storm of March 23–24, 2023, using 1) the spectrographic global survey method based on observational data from cosmic ray recording by the global network of stations (R_{sgs}); 2) numerical trajectory calculations in a model magnetic field of the magnetosphere (R_{eff}). The geomagnetic cutoff rigidity has been determined for nine cosmic ray stations at different latitudes. We calculated the correlations of the variations in the geomagnetic cutoff rigidity ΔR_{sgs} and ΔR_{eff} with magnetic and dynamic solar wind parameters and the geomagnetic activity indices *Dst* and K_p. It has been found that the geomagnetic cutoff rigidity calculated by both methods correlate most strongly with *Dst* and the electromagnetic parameters of the solar wind. No significant correlation with the dynamic parameters was observed. The analysis has shown that the response of ΔR_{sgs} to the controlling magnetic parameters and *Dst* changes with latitude of the observation station: the correlation reaches its highest values at midlatitudes and drops significantly toward the equator. The correlations of ΔR_{eff} calculated by the model do not reveal a latitudinal dependence.

Keywords: cosmic rays, geomagnetic threshold, cosmic ray cutoff rigidity, interplanetary magnetic field, geomagnetic activity.

INTRODUCTION

Under the influence of the geomagnetic field, charged particles of galactic cosmic rays (CRs) change their trajectory. Some of them with rigidity below the threshold value characteristic of the station that measures them (geomagnetic cutoff rigidity, R_c) do not reach Earth's surface. Due to the screening nature of the geomagnetic field, significantly fewer particles penetrate to the equator than to high latitudes. Variations in CR fluxes in the magnetosphere during magnetic storms are caused by changes in the CR geomagnetic cutoff rigidity/geomagnetic thresholds ΔR. The thresholds depend on the screening properties of the geomagnetic field.

During a magnetic storm, the solar wind (SW) energy is transferred to Earth's magnetosphere by coronal mass ejections (CMEs) or high-velocity corotating interaction regions (CIRs) from coronal holes. The influx of energy generated during increased solar activity and its subsequent attenuation in the magnetosphere determines the evolution of a geomagnetic storm, which is described by various geomagnetic indices. The K_p index — a planetary index characterizing the global geomagnetic disturbance within a three-hour time interval — is defined as average disturbance levels of two horizontal geomagnetic field components observed at 13 selected magnetic observatories located in the subauroral zone between 48° and 63° north and south geomagnetic latitudes. Another widely used one is the so-called disturbance storm time index *Dst*, which is calculated as the hourly average disturbance of the horizontal *H* component of the geomagnetic field at four low-latitude magnetic observatories. It is a measure of change in the magnetic field by the magnetopause current system (DCF) and the westward ring current (DR). The current system developed during a geomagnetic disturbance causes a decrease in the magnetospheric magnetic field and hence in geomagnetic screening, thereby facilitating penetration of CRs to lower latitudes. In turn, the dynamics of current systems depends on the dynamics of magnetic and time-varying parameters of near-Earth space.

Knowledge of the dependences of ΔR on SW and magnetosphere parameters can shed light on important features of the SW– magnetosphere coupling and its associated geomagnetic effects, which control CR transport through the magnetosphere and atmosphere during disturbances. Studying latitude effects of this coupling is essential for safety of the crew and passengers of space flights, as well as high-latitude and altitude flights [Burov et al., 2005; Iucci et al., 2005].

The response of geomagnetic screening to changes in the geomagnetic conditions in SW and the interplanetary magnetic field (IMF) during magnetic storms has

been examined theoretically and experimentally in [Kanekal et al., 1998; Leske et al., 2001; Shimazu, 2009; Tyssøy and Stadsnes, 2014; Adriani et al., 2016]. However, no definitive answer has been found yet to the question as to which near-space parameters control CR transport during disturbances. To answer this question, it is necessary, at least, to have a sufficiently extensive base of relevant data for geomagnetic storms of various types and intensities from different sources on the Sun and in interplanetary space, which occurred during different solar cycle phases. The data would allow us to draw generalized conclusions about changes in geomagnetic screening during interplanetary and geomagnetic disturbances of various types. Earlier in [Ptitsyna et al., 2019; Danilova et al., 2023 and references there], for one moderate and seven strong geomagnetic storms of solar cycles 23 and 24, we have calculated geomagnetic cutoff rigidities and their correlations with helio- and geosphere parameters. Most of the storms considered were recorded during descending phases and solar minima. In this paper, to further expand our data archive, we analyze the severe storm in March 2023 near the maximum of cycle 25, caused by specific stealth CME. Besides, we have added to our study the calculation and analysis of data for three additional low-latitude CR stations, bearing in mind the search for latitude effects. The purpose of this work is to identify geomagnetic thresholds, using two independent methods R_{eff} and R_{shs} during the March 23–24, 2023 severe storm, to analyze the dependence of their changes on the interplanetary medium and geomagnetosphere parameters, focusing on latitudinal effects, as well as to compare results obtained by different methods. To solve these problems, we calculated correlations of variations in geomagnetic cutoff rigidities ΔR_{sgs} and ΔR_{eff} with SW electromagnetic and dynamic parameters, *Dst*, and K_p.

1. METHODS AND DATA

The spectrographic global survey (SGS) method and the method of tracing trajectories of CR particles in a model magnetic field have been employed to calculate the geomagnetic cutoff rigidity during the severe magnetic storm on March 23–24, 2023.

The SGS method is based on the assumption that CR flux variations on Earth's surface are determined by the rigidity spectrum, the pitch-angle distribution of particles in interplanetary space, and the particle density gradient at the Larmor radius [Kovalev et al., 2022]. This method provides information on the distribution of primary CRs by energy and pitch angles in interplanetary space, as well as on changes in the planetary system of geomagnetic cutoff rigidities for each moment of observations (R_{sgs}), from ground-based observations of CRs made at the worldwide network of stations.

Table 1 lists standard errors in determining the IMF longitude λ and latitude Ψ angles, the differential rigidity spectrum A_0, CR pitch-angle anisotropy amplitudes A_1 and A_2, variations in the geomagnetic cutoff rigidity ΔR_c, surface ΔT_{SL} and mass average ΔT_{MA} atmospheric temperatures by the SGS method in accordance with the accuracy of measurements of CR neutron I_{nm} and charged I_{mt} components.

The statistical error in determining ΔR_{sgs} with due regard to the accuracy of measurements at CR stations does not exceed 0.05 GV in absolute value. The geomagnetic cutoff rigidity variations obtained by this method are further referred to as observed.

The second method involves trajectory calculations of R_c [Shea et al., 1965] in the model magnetic field of the magnetosphere (R_{eff}). In this paper, we employ the Tsyganenko model *T*s01 ([Tsyganenko et al., 2003] and references there) to compute the effective geomagnetic thresholds R_{eff}. At the same time, the accuracy of determining geomagnetic thresholds depends on the accuracy of the magnetospheric model adopted for calculations. According to the *T*s01 model, the magnetic field inside the magnetosphere (without the main magnetic field) is the sum of contributions from the main magnetospheric current systems. In parameterizing the current systems, we have used satellite data collected during 37 geomagnetic storms with *Dst*<–65 nT [Tsyganenko et al., 2003]. The *T*s01 model includes Chapman—Ferraro currents, symmetric and partial volume circular currents, transverse tail currents, and large-scale field-aligned currents. Tyasto et al. [2012] have shown that during strong magnetic storms the *T*s01 magnetospheric model describes the situation in the magnetosphere better than the *T*s04 model. To calculate the magnetic field from internal sources, a representation of Earth's main magnetic field (EMMF) is utilized as expansion in terms of spherical harmonic functions up to n=10. The geomagnetic cutoff rigidity variations obtained by this method are further referred to as model.

Table 1

Standard errors in IMF, CR, Earth's magnetosphere and atmosphere parameters, determined by the SGS method in accordance with the accuracy of neutron monitor and muon telescope data [Kovalev et al., 2022]

I_{nm}, %	I_{mt}, %	λ, deg.	Ψ, deg.	A_0, %	A_1, %	A_2, %	ΔR_c, GV	T_{SL}, °C	T_{AM}, °C
±0.1	±0.1	±16.9	±21.5	±1.0	±8.8	±1.7	±0.03	±1.3	±0.3
	±0.2	±16.9	±21.5	±1.0	±8.8	±1.7	±0.03	±2.5	±1.2
±0.15	±0.1	±17.0	±21.8	±1.3	±8.8	±1.7	±0.04	±1.3	±0.3
	±0.2	±17.0	±21.8	±1.3	±8.8	±1.7	±0.04	±2.5	±1.0
±0.2	±0.1	±17.5	±22.1	±1.6	±8.9	±1.8	±0.05	±1.3	±0.3

Geomagnetic cutoff rigidities have been determined for nine multi-latitude CR stations, listed in Table 2. The stations were chosen in such a way that under quiet conditions they covered the main range of threshold R_c affected by the geomagnetic field.

Next, we calculated the correlation coefficients k and the standard errors s between ΔR_{eff} and ΔR_{sgs} with the following parameters: IMF's total value B and its components B_z and B_y, the azimuthal component of electric field E_y, the plasma parameter β, SW velocity V, density N, and pressure P, as well as Dst and K_p. These parameters are available in the OMNI database [https://omniweb.gsfc.nasa.gov/form/dx1.html].

Plasma β is the ratio of plasma pressure to magnetic pressure; in the OMNI database, this parameter is calculated using the formula

$$\beta = \left(4.16T/10^5 + 5.34\right) N_p / B^2,$$

where T is the temperature (K); N_p is the proton density (cm^{-3}); B is the total magnetic field (nT).

The electric field was calculated by the formula

$$E = -VB_z 10^{-3},$$

where E is the electric field (mV/m); V is the proton velocity (km/s); and B_z is the magnetic field component (nT).

Table 2

Cosmic ray stations

Station name	International code	Geographic latitude	Geographic longitude	R_c
Kingston	KGSN	42.99° S	147.29° E	1.9
Moscow	MOSC	55.47° N	37.32° E	2.08
Novosibirsk	NVBK	54.80° N	83.00° E	2.32
Irkutsk	IRKT	52.47° N	104.03° E	3.13
Jungfraujoch	JUNG	46.55° N	7.98° E	4.51
Almaty	AATB	43.25° N	76.92° E	5.21
Rome	ROME	41.90° N	12.52° E	6.11
Athens	ATHN	37.97° N	23.72° E	8.48
Emilio Segre Obs.	ESOI	33.30° N	35.80° E	10.73

2. RESULTS

2.1. Helio-, geosphere parameters and CR cutoff rigidity during the March 23–24, 2023 storm

In Figure 1 from top to bottom are electromagnetic and dynamic parameters of SW and geomagnetic activity during the March 23–24, 2023 geomagnetic storm: B, B_z, E_y, β, SW V, N, P, as well as K_p and Dst.

A peculiarity of the storm under study was that it was caused by stealth CME. Such CMEs are not associated with any visible manifestations on the Sun, so it is difficult to identify them and hence to predict their geoeffectiveness. In particular, the CME that initiated the geomagnetic storm of interest was not observed by any of the observers and was not cataloged. However, since the peak Dst index unexpectedly reached –163 nT, the storm was classified as severe [Tahir et al., 2024; Teng et al., 2024].

On March 23 at ~8:00–14:00 UT, B, N, P, and B_z are seen to gradually increase, which can be interpreted as the passage of interplanetary CME sheath (ICME sheath) or compression region before ICME near Earth.

It can be assumed that the main phase of the storm began at ~13:00 UT with a sharp compression of the magnetosphere after a jump in P to 14.8 nPa. With the beginning of the main phase, β decreased abruptly from the background β≈2 before the storm to β≈0.2 and remained so throughout the main phase of the storm. Such a low β value may be associated with increased plasma turbulence and serve as a trigger for a magnetic storm [Kurazhkovskaya et al., 2021]. The B_z component fluctuated between southward and northward before finally turning south at ~18:00 UT. At that time, the active stage of the storm began when Dst started to decrease sharply and reached a minimum (Dst=–163 nT) at 02:00 UT on March 24, 2023. After that, Dst began to increase, B_z also began to grow, and the magnetic storm entered the relaxation phase.

Figure 2, *a*–*f* presents calculated variations in the geomagnetic thresholds ΔR_{sgs} and ΔR_{eff} for all the stations considered. Panel *g* also shows Dst variations to illustrate the relationship between dynamics of the geomagnetic thresholds and evolution of the storm. The trend of the ΔR_{eff} and ΔR_{sgs} curves is seen to agree well with Dst.

There is a clear dependence of lowering the ΔR_{eff} thresholds on latitude. The value of ΔR_{eff} reached its maximum drop (≈–0.8 GV) during the main phase at the storm maximum (Dst=–163 nT) at the station with the lowest threshold rigidity R_c (KGSN).

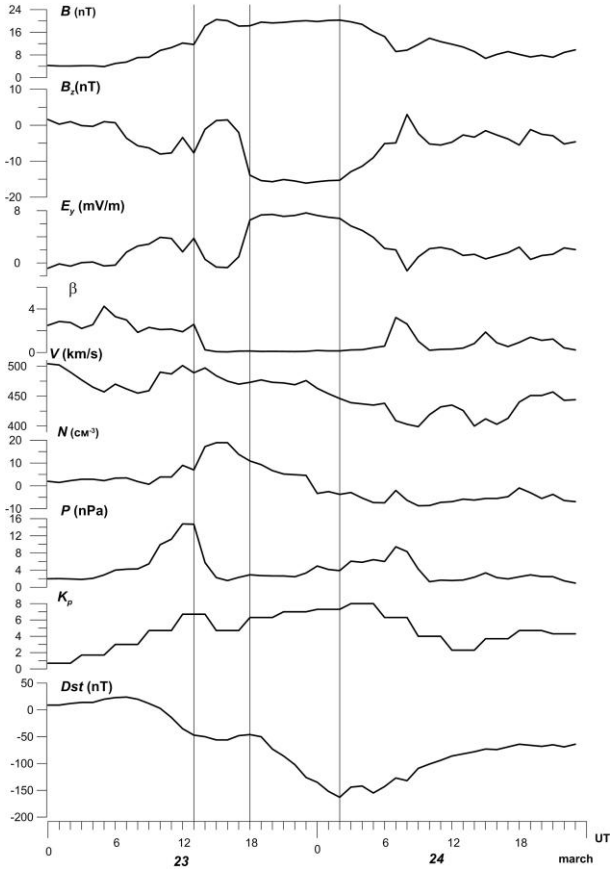

Figure 1. Parameters of SW, IMF, and geomagnetic activity during the storm on March 23–24, 2023. Vertical lines indicate the storm main phase, as well as the beginning of the active stage of the main phase at ~18:00 UT on March 23

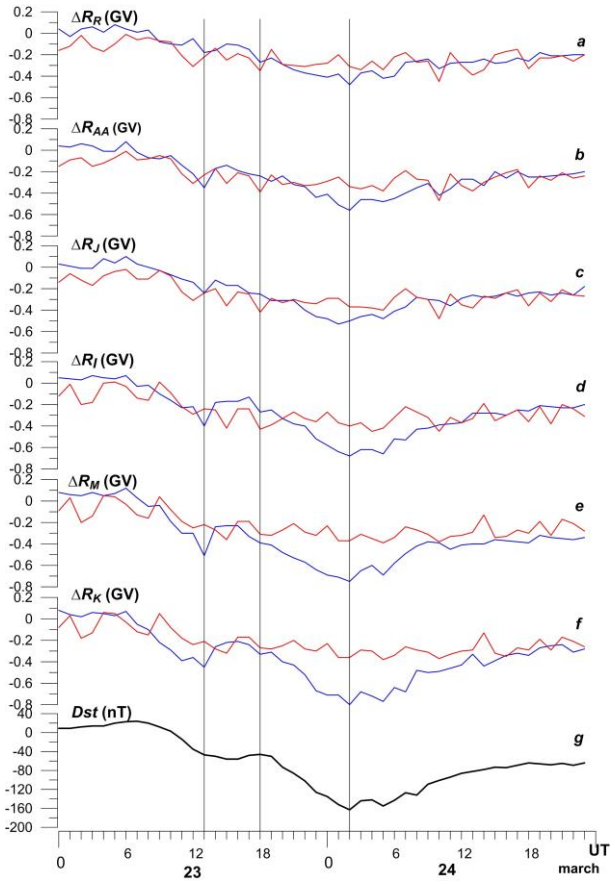

Figure 2. Variations in geomagnetic thresholds ΔR_{sgs} (red lines) and ΔR_{eff} (blue lines) during the September 23–24, 2023 storm. From top to bottom for ROME (*a*), AATB (*b*), JUNG (*c*), IRKT (*d*), MOSC (*e*), and KGSN (*f*). Panel (*g*) is the *Dst* index. Vertical lines indicate the storm main phase and the onset of the active phase (18:00 UT on March 23)

During the storm main phase, ΔR_{sgs} decreases more slowly and to a smaller extent than ΔR_{eff}. In addition, oscillations with a period of about several hours are superimposed on the general trend of ΔR_{sgs}, which follows *Dst*. Amplitude of these oscillations during the recovery phase is of roughly the same order as the decrease in ΔR_{sgs} near the storm maximum: (for example, 2 hrs after the storm maximum at IRKT, ΔR_{sgs}=–0.45 GV). Such jumps in ΔR_{sgs} are especially characteristic for the storm recovery phase at low-latitude stations. It is, therefore, impossible to determine with sufficient accuracy the maximum drop in geomagnetic cutoff rigidity during the storm. We can only note that along with the evolution of the ring current (~30 hrs for this storm), which determines ΔR_{eff}, other shorter-period (~2–3 hrs) processes seem to make a significant contribution. Figure 2 also demonstrates that the difference between the ΔR_{eff} and ΔR_{sgs} curves depends on latitude. It has a 0.44 GV maximum during minimum *Dst* for KGSN with minimum R_c=1.90 GV.

2.2. Correlation analysis

The time curves of Figure 2 suggest that ΔR_{eff} and ΔR_{sgs} vary with evolution of the storm and hence with changes in SW and geomagnetic activity parameters. In order to quantify the relationship between the parameters and the variations in geomagnetic thresholds, we have analyzed the correlations of ΔR with the SW, IMF parameters and the geomagnetic activity indices. Correlation coefficients *k* and standard errors *s* were calculated. Figure 3 plots the correlation *k* between ΔR and the SW, IMF, and geomagnetosphere parameters during the March 23–24, 2023 storm. Panel *a* illustrates the correlation of variations in model thresholds ΔR_{eff} with interplanetary and magnetic parameters; panel *b*, the correlation between observed ΔR_{sgs}. Columns of the diagrams in different colors correspond to the results of the correlation analysis for different stations. The columns (stations) are arranged in ascending order of latitude (decreasing station threshold under quiet conditions).

Panel *a* shows that the greatest correlation is observed between ΔR_{eff} and *Dst*. For ΔR_{eff}, k=0.96±0.05 at YUNG. At other stations, *k* is almost the same. A high but somewhat lower negative correlation is also seen for K_p. For example, at MOSC k=–0.8±0.14. The correlation close to k=–0.8 was obtained for the relationship between the model geomagnetic thresholds and the general magnetic field *B*. At MOSC, k=–0.74±0.16; at ESOI, k=–0.7±0.08. In this case, k<0. A high anticorrelation was also derived for the relationship with E_y: k=–0.68±0.18 at MOSC. Similar *k* values were also found for the other stations. A fairly high correlation of about the same order ~0.65–0.7 was

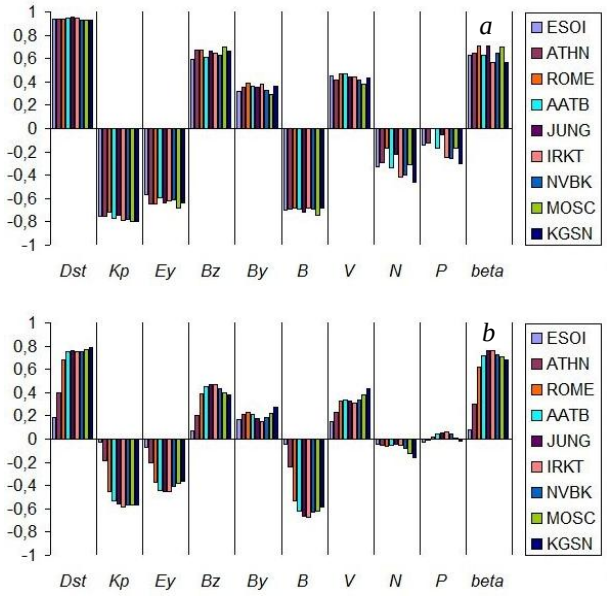

Figure 3. Correlation coefficients k between cutoff rigidities and geo- and heliosphere parameters during the March 23–24, 2023 storm: ΔR_{eff} (*a*); ΔR_{sgs} (*b*)

obtained for β and B_z. Note that the relationship of ΔR_{eff} with B_z is weaker than with the total field B. The k value is much smaller for the correlation between ΔR_{eff} and B_y. For example, k=0.39±0.14 at ROME. The k value calculated for the correlation ΔR_{eff}–V is of the same order and even smaller for the anticorrelation ΔR_{eff}–N and ΔR_{eff}–P. It can be argued that variations in geomagnetic cutoff rigidities are most closely related to variations in geomagnetic activity indices. Moreover, all electromagnetic parameters, except for B_y, contribute substantially to threshold variations. As for the SW dynamic parameters, the relationship with them is insignificant. Note that the coefficients of correlation ΔR_{eff} with all parameters calculated for different stations differ very little.

A slightly different pattern is observed for the variation in threshold rigidities obtained by the SGS method (panel *b*). In general, the correlation coefficients for observed ΔR_{sgs} are lower than for model ΔR_{eff}. The closest correlation for mid-latitude stations is observed between ΔR_{sgs} and *Dst*, as well as β, reaching almost 0.8. The k value is the largest for KGSN (0.79±0.07). There is almost no correlation with *Dst* at the low-latitude stations ESOI and ATHN. The same can be said about the relationship of ΔR_{sgs} with the total magnetic field B and β. The correlation ΔR_{sgs}–β is the closest at the mid-latitude stations JUNG and IRKT (k=0.76±0.08), and for ΔR_{sgs}–B k=–0.67±0.09. For the other parameters, the correlation is much lower, and it is absent for the SW dynamic parameters N and P.

2.3. Correlations of geomagnetic thresholds with SW, IMF, and geomagnetic activity parameters

Figure 4 illustrates the relationship between variations in geomagnetic thresholds ΔR and the SW, IMF, geomagnetic activity parameters under study as function of geomagnetic cutoff rigidities R_c of stations under quiet conditions. The k values are shown for ΔR_{eff} (*a*) and ΔR_{sgs} (*b*). Colors and symbols denote the curves related to *Dst*, K_p, B_z, E_y, B_y, P, B, β, V, and N. Curves in panels *a*, *b* confirm the conclusions, obtained from the diagrams (see Figure 3, *a*, *b*), that the closest correlation is observed between ΔR_{sgs} and *Dst*, β; a slightly less close one, with B_z; and the greatest anticorrelation, with B, K_p, and E_y. Besides, panel *b* demonstrates the dependence of k on latitude and hence on R_c. The closest correlation is seen at midlatitudes for which R_c≈2÷6 GV; and the maximum, at IRKT and JUNG for which R_c=3.13 and 4.51 respectively. With an increase in R_c>6 GV, k decreases significantly. For the other parameters considered, k is small, so they are not geoeffective and can be ignored.

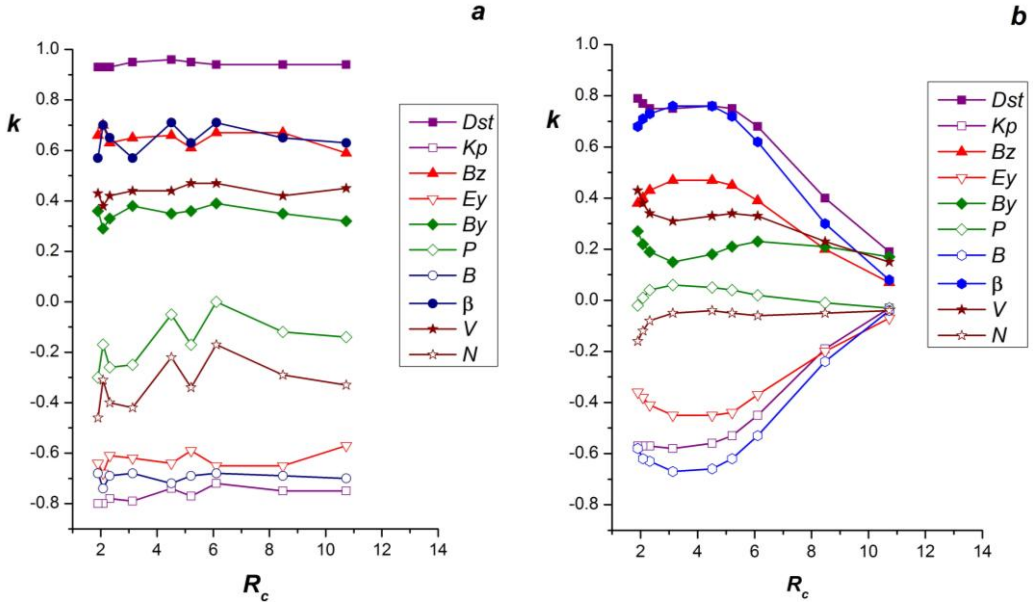

Figure 4. Correlation coefficients k between geomagnetic cutoff rigidities and geo- and heliospheric parameters depending on latitude: ΔR_{eff} (*a*); ΔR_{sgs} (*b*)

For ΔR_{eff} (*a*), the strongest correlation and anticorrelation (see Figure 3, *a*) are found for the same parameters as for ΔR_{sgs} — with *Dst*, β, B_z, K_p, *B*, and E_y. However, *k* for all parameters of the correlation ΔR_{eff} is higher than for ΔR_{sgs}. As for the latitude dependence, a weak trend similar to the latitude effect in ΔR_{sgs} can be detected only for B_z and E_y. For the other parameters under study, there is almost no dependence on latitude. Here, we also discuss only geoeffective parameters for which *k* is large enough.

2.4. Correlation between ΔR_{eff} and ΔR_{sgs}

Let us compare the results obtained by the SGS method and trajectory calculations using the Ts01 model. To do this, we calculated the correlation *k* between ΔR_{eff} and ΔR_{sgs} (Table 3).

Analysis of Figures 3, 4 shows that ΔR_{eff} and ΔR_{sgs} in general similarly describe variations in thresholds during the storm and the contribution of helio- and geosphere parameters to these variations. This is despite the fact that the drop in the model thresholds ΔR_{eff} systematically exceeds the drop in the observed ones ΔR_{sgs}. Table 2 suggests that the correlation *k* during the storm under study between observed and model thresholds for all stations, except for ESOI and ATHN, is quite high: from k=0.71±0.07 for ROME to the correlation maximum k=0.78±0.07 for JUNG. This behavior of *k* indicates a similar sensitivity to interplanetary and geomagnetic parameters of observed and model variations in geomagnetic thresholds for the stations with R_c<6.11 GV (ROME). The low correlation between ΔR_{eff} and ΔR_{sgs} at ESOI and ATHN reflects the difference in the latitude effect noticeable at low-latitude stations (see 2.3).

Table 3

Correlation coefficients *k* between ΔR_{eff} and ΔR_{sgs}

	ESOI	ATHN	ROME	AATB	JUNG	IRKT	NVBK	MOSC	KGSN
k	0.14±0.13	0.42±0.1	0.71±0.07	0.76±0.07	0.78±0.07	0.71±0.09	0.76±0.08	0.77±0.08	0.73±0.08

CONCLUSIONS

In this paper, we have examined variations in geomagnetic cutoff rigidities ΔR_{eff} and ΔR_{sgs} during the March 23–24, 2023 storm, which were calculated by two different methods, observational and model. In addition, we have analyzed the relationship of these variations with electromagnetic and dynamic parameters of solar wind and geomagnetic activity, as well as the dependence of this relationship on latitude.

It has been found that the geomagnetic thresholds calculated by both methods correlate most strongly with geomagnetic activity, especially with *Dst*, which indicates the greatest contribution to variations of ring current rigidities. Besides, there is a high correlation with electromagnetic parameters of IMF *B*, β, B_z, E_y. There is no significant correlation with the SW dynamic parameters *V*, *N*, *P*. It is believed that the development of a magnetic storm mainly depends on two parameters: the IMF southward component whose growth leads to reconnection of the SW magnetic field and Earth's magnetosphere, and on the SW pressure *P* whose rise results in the compression of the magnetosphere [Dungey, 1961; Burton et al., 1975; Akasofu, 1984]. However, the development of the storm under study and hence a decrease in geomagnetic screening during the storm and geomagnetic cutoff rigidity variations were indeed determined by B_z and, to an even greater extent, by the total magnetic field *B* and the plasma parameter β, whereas *P* and the other dynamic parameters of SW practically played no role. Note that such results were obtained for a severe storm in March 2023, i.e. on the ascending branch of solar cycle 25, one and a half years before its maximum. These results are generally consistent with the conclusions about the predominant influence of *Dst* and some electromagnetic parameters on Δ*R*, drawn for the March 8–11, 2012 strong storm also on the ascending branch of solar cycle 24 two years before the maximum [Danilova et al., 2023]. At the same time, for most storms, largely recorded outside solar maximum [Ptitsyna et al., 2019], along with the constant strongest correlation with *Dst* and electromagnetic parameters there is a significant relationship between geomagnetic thresholds and SW velocity. In this case, sets of other control parameters for individual storms differ. Nevertheless, we can conclude that properties of geomagnetic screening during strong disturbances depend on the phase of the solar cycle in which the event occurred. However, these conclusions need further, more detailed verification.

Analysis has shown that the response of ΔR_{sgs} to the controlling electromagnetic parameters, as well as to *Dst* and K_p, varies with the latitude of the observation station: the correlation reaches its highest values at midlatitudes (R_c≈2÷6 GV) and decreases significantly toward the equator. Practically no latitude dependence has been found for the correlations of ΔR_{eff} with interplanetary and geomagnetic parameters, only the correlation of ΔR_{eff} with B_z and E_y demonstrates a similar but weaker latitude effect.

Despite the difference in the magnitude and behavior of *k*, at low-latitude stations the correlation between ΔR_{eff} and ΔR_{sgs} as a whole is quite high (0.7). This suggests that both methods in use adequately describe Δ*R* in terms of variations in geomagnetic and interplanetary parameters at midlatitudes. The difference between the effects obtained by these methods at low-latitude stations should be investigated further.

We are grateful for the opportunity to use the OMNI database [http://omniweb.gsfc.nasa.gov]. The work was partially carried out with the financial support from the Ministry of Science and Higher Education of the Russian Federation (Subsidy No. 075-GZ/Ts3569/278). The results

for ΔR_{sgs} were obtained using the equipment of Shared Equipment Center "Angara" [http://ckp-rf.ru/ckp/3056/] and the Unique Research Facility "Russian National Ground-Based Network of Cosmic Ray Stations" (CRS network) [https://ckp-rf.ru/usu/433536].

REFERENCES

Adriani O., Barbarino G.C., Bazilevskaya G.N., Bellotti R., Boezio M., Bogomolov E.A., et al. PAMELA's measurements of geomagnetic cutoff variations during the 14 December 2006 storm. *Space Weather*. 2016, vol. 14, no. 3. DOI: 10.1002/2016SW001364.

Akasofu S.-I. The magnetospheric currents: An introduction. In T.A. Potemra (Ed.), Magnetospheric currents. *Geophysical Monograph Series*. 1984, vol. 28, pp. 29–48. DOI: 10.1029/GM028p0029.

Burov V.A., Meleshkov Yu.S., Ochelkov Yu.P. The technique of operational evaluation of the level of radiation danger due to the cosmic weather disturbance during air travel. *Heliogeophysical Research.* 2005, iss. 7, pp. 1–41.

Burton R.K., McPherron R.L., Russell C.T. An empirical relationship between interplanetary conditions and *Dst. J. Geophys. Res*. 1975, vol. 80, iss. 31, pp. 4204–4214. DOI: 10.1029/JA080i031p04204.

Danilova O.A., Ptitsyna N.G., Tyasto M.I., Sdobnov V.E. Variations in cosmic ray cutoff rigidities during the March 8–11, 2012 magnetic storm (CAWSES II period). *Sol.-Terr. Phys.* 2023, vol. 9, iss. 2, pp. 81–87. DOI: 10.12737/stp-92202310.

Dungey J.W. Interplanetary magnetic field and the auroral zones. *Phys Rev Lett.* 1961, vol. 6, pp. 47–48. DOI: 10.1103/ PhysRevLett.6.47.

Iucci N., Levitin A.E., Belov A.V., Eroshenko E.A., Ptitsyna N.G., Villoresi G., et al. Space weather conditions and spacecraft anomalies in different orbits. *Space Weather*. 2005, vol. 3, S01001. DOI: 10.1029/2003SW 000056.

Kanekal S., Baker D., Blake J., Klecker B., Cummings J., Mewaldt R., Mason G., Mazur J. High-latitude energetic particle boundaries and the polar cap: A statistical study. *J. Geophys. Res.: Space Phys.* 1998, vol. 103, pp. 9367–9372.

Kovalev I.I., Olemskoy S.V., Sdobnov V.E. A proposal to extend the spectrographic global survey method. *J. Atmos. Solar-Terr. Phys.* 2022, vol. 235, p. 105887. DOI: 10.1016/ j.jastp.2022.105887.

Kurazhkovskaya N.A., Zotov O.D., Klain B.I. Relationship between geomagnetic storm development and the solar wind parameter β. *Sol.-Terr. Phys*. 2021, vol. 7, no. 4, pp. 25–34. DOI: 10.12737/szf-74202104.

Leske R.A., Mewaldt R.A., Stone E.C., von Rosenvinge T.T. Observations of geomagnetic cutoff variations during solar energetic particle events and implications for the radiation environment at the space station. *J. Geophys. Res*. 2001, vol. 106, pp. 30011–30022. DOI: 10.1029/2000JA000212.

Ptitsyna N.G., Danilova O.A., Tyasto M.I., Sdobnov V.E. Influence of the solar wind and geomagnetic activity parameters on variations in the cosmic ray cutoff rigidity during strong magnetic storms. *Geomagnetism and Aeronomy*. 2019, vol. 59, no. 5, pp. 530–538. DOI: 10.1134/S001679321905 0098.

Shea M.A., Smart D.F., McCracken K.G. A study of vertical cutoff rigidities using sixth degree simulations of the geomagnetic field. *J. Geophys. Res*. 1965, vol. 70, pp. 4117–4130.

Shimazu H. Solar proton event and proton propagation in the Earth's magnetosphere. *J. National Institute of Information and Communications Technology*. 2009, vol. 1, pp. 191–199.

Tahir A., Wu F., Shah M., Amory-Mazaudier C., Jamjareegulgarn P., Verhulst T.G.W., Ayyaz Ameen M. Multi-instrument observation of the ionospheric irregularities and disturbances during the 23–24 March 2023 geomagnetic storm. *Remote Sensing.* 2024, vol. 16, no. 9, p. 1594. DOI: 10.3390/rs16091594.

Teng W., Su Y., Ji H., Zhan Q. Unexpected major geomagnetic storm caused by faint eruption of a solar transequatorial flux rope. *Nature Communications*. 2024, vol. 15, pp. 9198–9214. DOI: 10.1038/s41467-024-53538-1.

Tsyganenko N.A., Singer H.J., Kasper J.C. Storm-time distortion of the inner magnetosphere: How severe can it get? *J. Geophys. Res*. 2003, vol. 108, no. A5, p. 1209. DOI: 10.1029/2002JA009808.

Tyasto M.I., Danilova O.A., Sdobnov V.E. Cosmic ray geomagnetic cutoff rigidities in the magnetic field of two empirical models during a strong disturbance in November 2003: A comparison of models. *Geomagnetism and Aeronomy.* 2012, vol. 52, pp. 1087–1096. DOI: 10.1134/S0016793212080208.

Tyssøy H.N, Stadsnes J. Cutoff latitude variation during solar proton events: Causes and consequences. *J. Geophys. Res. Space*. 2014, vol. 120, pp. 553–563. DOI: 10.1002/2014JA 0200508.

URL: https://omniweb.gsfc.nasa.gov/form/dx1.html (accessed January 16, 2024).

URL: http://omniweb.gsfc.nasa.gov (accessed January 16, 2024).

URL: http://ckp-rf.ru/ckp/3056/ (accessed January 16, 2024).

URL: https://ckp-rf.ru/usu/433536 (accessed January 16, 2024).

The paper is based on material presented at the 20th Annual Conference on Plasma Physics in the Solar System, February 10–14, 2025, Space Research Institute of the Russian Academy of Sciences, Moscow, Russia.

Original Russian version: Danilova O.A., Ptitsyna N.G., Sdobnov V.E., published in Solnechno-zemnaya fizika. 2025, vol. 11, no. 3, pp. 42–49. DOI: 10.12737/szf-113202505.

How to cite this article

Danilova O.A., Ptitsyna N.G., Sdobnov V.E. Geomagnetic cutoff of cosmic rays during the March 23–24, 2023 magnetic storm: Relationship with solar wind parameters and geomagnetic activity taking into account latitudinal effects. *Sol.-Terr. Phys*. 2025, vol. 11, iss. 3, pp. 37–43. DOI: 10.12737/stp-113202505.